Apical Loop−Internal Loop Interactions: A New RNA−RNA Recognition Motif Identified through in Vitro Selection against RNA Hairpins of the Hepatitis C Virus mRNA†

Lydia Aldaz-Carroll,‡,§ Béatrice Tallet,‡,§ Eric Dausse,‡,§ Ludmila Yurchenko,‡,|| and Jean-Jacques Toulmé*,‡,§

INSERM U386, Université Victor Segalen, 146 rue Léo-Saignat, 33076 Bordeaux, France, and Institut Européen de Chimie et Biologie, Pessac, France

Received December 12, 2001; Revised Manuscript Received February 25, 2002

ABSTRACT: We performed in vitro selection of oligoribonucleotides in order to identify high-affinity motifs recognizing RNA hairpins located at the 3′ end (SL1) and at the 5′ end (domain IV of the internal ribosome entry site) of the hepatitis C virus mRNA. We selected aptamers constituted by an internal loop complementary to the SL1 apical loop, flanked by G-C-rich double-stranded regions, able to form complexes with a K_d of 70 nM, at 37 °C under ionic conditions close to intracellular ones. The complex involves selective apical loop (SL1)−internal loop (aptamer) interactions. Similar structurally organized aptamers were independently identified against domain IV and were shown to also give rise to such complexes. Apical loop−internal loop interaction could constitute a new recognition motif allowing specific intra- or intermolecular RNA−RNA association.

Numerous RNA structures present a regulatory function through interaction either with proteins or with nucleic acids. For instance, the bacteriophage R17 coat protein or the *Saccharomyces cerevisiae* L30 ribosomal protein autoregulate their production by binding to particular structured motifs on their own mRNA (*1*, *2*); the replication of the ColE1 plasmid of *Escherichia coli* is regulated by the interaction of two RNA transcripts, RNA I and RNA II (*3*).

High-affinity ligands that can recognize a structured RNA may prevent the interaction of the RNA with a regulatory partner, therefore interfering with the regulatory processes it mediates. This recognition can be achieved by the use of antisense oligomers (*4*); however, the thermodynamic penalty for unfolding the targeted RNA structure may prevent the formation of the sense−antisense duplex. Combinatorial strategies offer an alternative and powerful way to identify nucleic acid ligands (*5*, *6*). In vitro selection has been successfully used in our laboratory to identify DNA or RNA aptamers exhibiting high affinity for an RNA structure (*7*, *8*).

We decided to employ in vitro selection (SELEX) to identify RNA ligands of two untranslated domains of the hepatitis C virus (HCV)[1] mRNA: the 3′X element located in the 3′ untranslated region (UTR) and the internal ribosome entry site (IRES) corresponding to the 5′ end of viral mRNA (Scheme 1). The 3′X RNA structure, a 98 nt long region, has the potential to form three stem−loop structures, including a highly stable stem−loop of 46 nt at the very 3′ end named SL1 (*9*−*12*). RNA elements present within the 3′-terminal structures of other *Flaviviridae* members may represent cis regions crucial for viral replication (*13*, *14*). Although the importance of different conserved elements of the 3′UTR of HCV mRNA has not been established experimentally, many studies suggest that this region may play a critical role in RNA replication and translation. Indeed, the 3′X region is very conserved and has a stable secondary structure. It has been proposed that it may be involved in viral RNA synthesis (*10*, *11*, *15*). Interestingly, further studies have shown that the 3′X RNA is a minimal cis-acting sequence required for HCV minus-strand RNA synthesis and can be used as a template for in vitro RNA synthesis (*16*). It has also been proven that the 3′X region specifically enhances the IRES-dependent translation of HCV mRNA (*17*). In addition, deletion of large segments of the conserved part of the 3′UTR prevented the replication of an infectious cDNA clone of HCV in a chimpanzee (*18*).

The IRES, which represents the most conserved region of the HCV genome (*19*), mediates viral translation in a cap-independent manner (*20*). The predicted secondary structure of the HCV 5′UTR deduced from ribonuclease mapping, mutational analysis, and phylogenetic comparison shows four major structural domains. The stem−loop I had been previously shown as not being essential for IRES activity

† L.A.-C. was supported by a joint financing from the Foundation La Caixa (Spain) and the French Embassy in Madrid and by a research grant from the Association pour la Recherche contre le Cancer (France). L.Y. was the recipient of a PAST position. This work was supported by a grant from the Réseau Fondamental Hépatite C and by a concerted action (Picasso) between France and Spain.

* Correspondence to this author at INSERM U386, Laboratoire de Biophysique Moléculaire, 146 rue Léo-Saignat, 33076 Bordeaux, France. Tel: 33-557-57-10-14. Fax: 33-557-57-10-15. E-mail: Jean-Jacques.Toulme@bordeaux.inserm.fr.

‡ INSERM U386, Université Victor Segalen.

§ Institut Européen de Chimie et Biologie.

|| Present address: Supratek, Montréal, Canada.

[1] Abbreviations: HCV, hepatitis C virus; UTR, untranslated region; EMSA, electrophoretic mobility shift assay; nt, nucleotide; SPR, surface plasmon resonance.

10.1021/bi0121508 CCC: $22.00
Published on Web 04/16/2002

Scheme 1: HCV mRNA[a]

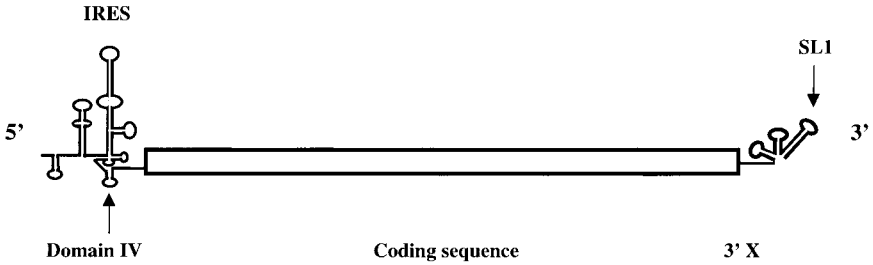

[a] The coding sequence (boxed) is flanked by the IRES and the 3′X. Domain IV of the IRES and the SL1 hairpin, which have been used for selection, are indicated.

(*20*−*22*). In contrast, domains II, III, and IV, which contains the translation start codon in the apical loop, as well as a pseudoknot motif are required for efficient initiation of viral translation (*21*, *23*, *24*).

In the present study, we performed an in vitro selection of oligoribonucleotides against the SL1 hairpin of the 3′X element in order to get selective high-affinity ligands of this structure which might be a useful tool for investigating the role played by the 3′X motif (Scheme 1). An aptamer showing an affinity of 70 nM at 37 °C was selected. This aptamer is an RNA hairpin with an internal loop which contains a sequence complementary to the top part of the target SL1 RNA. The SL1−aptamer complex involves an apical loop−internal loop (ALIL) interaction. In contrast to previous selections performed with RNA or DNA libraries against RNA hairpins (*7*, *8*) for which hairpin aptamers giving rise to kissing complexes have been identified as the strongest ligands, hairpins targeted to the SL1 loop led to kissing complexes of low stability compared to ALIL complexes. Interestingly, similar RNA aptamers displaying an internal loop and giving rise to ALIL interactions were selected against domain IV of the HCV IRES (Scheme 1). We describe here such aptamers and the complexes formed with their respective targets, which might constitute a new mode of RNA−RNA interaction.

MATERIALS AND METHODS

Oligonucleotides. The 3′ biotinylated SL1 RNA hairpin (5′CUGCAGAGAGUGCUGAUACUGGCCUCUCUGCAG) and domain IV of the HCV IRES (5′CGCGUGCACCAUGAGCACGCG) were chemically synthesized on an Expedite 8909 synthesizer. The RNA random library used for selection was obtained by transcription (Ampliscribe T7 high yield transcription kit from TEBU) from a DNA library, synthesized by Eurogentec, containing 40 random nucleotides flanked by invariant primer annealing sites: 5′GTGTGACCGACCGTGGTGC-N40-GCAGTGAAGGCTGGTAACC. The library used for selection against domain IV of the IRES had identical invariant flanks, but the random region was only 30 nt long. Three different primers (Genset) were used: P20 (same polarity as the DNA pool), 5′GTGTGACCGACCGTGGTGC; 3′S (complementary to the 3′ end of the DNA library), 5′CTATAGGTTACCAGCCTTCACTGC; and 3′L (complementary to the 3′ end of the DNA library and containing the T7 transcription promoter), 5′TAATACGACTCACTATAGTTACCAGCCT. The variants of the RNA aptamers were chemically synthesized on an Expedite 8909 synthesizer.

In Vitro Selection. (a) Selection against SL1. Selection steps were performed at 37 °C in R buffer (20 mM HEPES, pH 7.3 at 20 °C, containing 20 mM sodium acetate, 140 mM potassium acetate, and 3 mM magnesium acetate) in a total volume of 200 μL. Prior to use, 500 pmol of the RNA pool was heated at 80 °C for 1 min and allowed to cool for 15 min at room temperature. The RNA pool was mixed once with streptavidin beads (150 μg of Dynabeads M-280 or 100 μg of Eurobio MPG streptavidin) previously equilibrated in R buffer for 10 min. RNA candidates not retained by the beads were then mixed with 10 pmol of 3′ biotinylated SL1 for 20 min. Next, streptavidin beads were added to the mixture, and the mixture was incubated for an additional 10 min. Unbound RNA was then removed, and the beads were washed twice with 100 μL of R buffer. The bound candidates were eluted from the target RNA by heating for 40 s at 75 °C in 50 μL of water.

(b) Selection against IRES Domain IV. This selection was performed at 23 °C in R buffer. Prior to use, the RNA pool (2 nmol) was heated at 80 °C for 1 min, then cooled at 4 °C for 1 min, and placed at room temperature for 5 min. The RNA pool was mixed with streptavidin beads equilibrated in R buffer as described above. RNA candidates not retained by the beads were then mixed with 20 pmol of 3′ biotinylated domain IV for 5 min. Then, streptavidin beads were added to the mixture, and the mixture was incubated for 5 min. Unbound RNA was removed, the beads were washed with R buffer, and the bound RNA was eluted as above.

(c) RNA Amplification, Cloning, and Sequencing. RNA candidates were copied into cDNA with 200 units of SuperScript II RNase H$^-$ reverse transcriptase (Life Technologies), 2 μL of which were used for 25 cycles of polymerase chain reaction (PCR) with 0.4 unit of Goldstar DNA polymerase from Eurogentec, with the P20 and 3′S primers. A second PCR reaction allowed the insertion of the T7 promoter using 10 μL of the previous PCR and primers P20 and 3′L. RNA candidates were obtained by in vitro transcription, after precipitation, of the PCR products with the Ampliscribe T7 high yield transcription kit from TEBU. The transcription products were purified by electrophoresis on 20% denaturing polyacrylamide gels and then used for the next selection cycle. After 10 cycles selected sequences were cloned using the TOPO TA cloning kit from Invitrogen and sequenced by using the dRhodamine Terminator Cycle sequencing kit from Perkin-Elmer, according to the manufacturers' instructions.

Electrophoretic Mobility Shift Assay. To evaluate the K_d (dissociation constant) of the complexes formed by the target RNA hairpins (SL1 and domain IV) and the different

FIGURE 1: Sequences of RNA aptamers selected against SL1 RNA. The complementary sequence of SL1 is shown on top for direct comparison with aptamer sequences. Selected sequences, classified in three different classes depending on their predicted secondary structure, are shown below. The part of the sequences complementary to the SL1 loop is boxed, whereas that complementary to the stem is colored in light gray. Arrows correspond to double-stranded stems. Numbers appearing under the left-hand column represent the aptamer name, followed by the multiplicity of selected sequences in parentheses. The second column from the left indicates the aptamer dissociation constant at 37 °C, evaluated by electrophoretic mobility shift assay (see Materials and Methods). The predicted secondary structure for each class is schematized to the right. The thick solid line indicates the consensus sequence.

aptamers, electrophoretic mobility shift assays (EMSA) were performed at the indicated temperature. One nanomolar of ^{32}P 5′end-labeled SL1 or domain IV was incubated with increasing concentrations of aptamer for 20 min in 10 μL of R buffer. Samples were run on a native gel [10% or 15% (w/v) 19:1 acrylamide/bisacrylamide] in 50 mM Tris−acetate (pH 7.3 at 20 °C) and 3 mM magnesium acetate at 80 V (4 V/cm) for 37 °C, 100 V (5 V/cm) for 20 °C, or 300 V (15 V/cm) for 4 °C for 15 h and quantified by Instant Imager analysis (Hewlett-Packard). K_d values were calculated from data point fitting using KaleidaGraph 3.0 (Abelbeck software), according to the equation [complex] = [RNA]-[aptamer]$_0$/[RNA + K_d], [RNA] being the concentration of free ^{32}P 5′-end-labeled target RNA hairpin, i.e., either SL1 or domain IV, and [aptamer]$_0$ corresponding to the total concentration of unlabeled aptamer.

RNase Probing of Complexes. RNase probing of the target hairpin/aptamer complexes was performed with either ^{32}P 3′-end-labeled aptamer or ^{32}P 5′-end-labeled target, as indicated. Prior to use, all RNAs were separately heated for 1 min at 100 °C, then cooled for 1 min at 4 °C, and allowed to reach room temperature for 5 min. Before digestion, the labeled RNA (10 nM) and the unlabeled partner or control molecule (over 500-fold excess) were hybridized in R buffer for 10 min at 23 °C for analysis of domain IV interactions or for 5 min at 37 °C for analysis of SL1 complexes (10 μL final volume). Then RNase T1 (50−500 milliunits) (Boehringer-Mannheim) or RNase A (20 or 50 pg) (Pharmacia-Biotech) was added. RNA digestion was performed for 10 min at 23 °C for analysis of domain IV interactions or at 37 °C for analysis of SL1 complexes, and a control aliquot of the RNA complex in the absence of RNases was processed in parallel to the digested samples. Reactions were stopped at 4 °C by the addition of 40 μL of a solution containing 5 μg of tRNA (Sigma-Aldrich) and ethanol precipitated in 0.3 M sodium acetate (pH 5.2). The pellet was resuspended in loading buffer (8 M urea, 0.1 M Tris, pH 8.4, 0.39 M boric acid, 0.3 M ethylenediaminetetraacetic acid, bromophenol blue, and xylene cyanol), and the cleavage products were analyzed on 20% denaturing polyacrylamide gels. RNA ladders were generated either by digestion of ^{32}P end-labeled RNA with RNase T1 in denaturing conditions (3.5 M urea, 18.4 mM sodium citrate) at 50 °C for 10 min or by alkaline hydrolysis at 90 °C for 15 min in 50 mM $NaHCO_3$ (pH 9.5).

Surface Plasmon Resonance Measurements. SPR experiments were performed with a BIAcore 2000 apparatus. Biotinylated miniTAR or SL1 (200−300 RU) was immobilized on different channels of the same CM5 sensorchip coated with strepatividin as described previously (*25*). Binding experiments were performed at 23 °C in R buffer. All oligonucleotides were prepared in this buffer at 1 μM, injected at a flow rate of 20 μL/min during 600 s, and allowed to dissociate for 15 min. When needed, ROP protein prepared as described previously (*26*) was mixed in the same buffer at 0.8 μM with the oligonucleotide at 1 μM and injected at the same flow rate during the last 300 s.

RESULTS

Selection against RNA Hairpin SL1. RNA aptamers that bind to the RNA hairpin SL1 present at the very 3′ end of the HCV RNA (sheme 1) were selected within a 40 nt randomized RNA library that contained 10^{13} different sequences. An excess of RNA candidates was incubated with the target at 37 °C in R buffer, i.e., under temperature and ionic conditions chosen to mimic intracellular ones (see Materials and Methods). The RNA−RNA complexes were captured by magnetic streptavidin beads as the RNA target was 3′ biotinylated. As a means to diminish the number of candidates that could be selected against the beads themselves, we included a counter-selection step against the naked beads and alternated the type of beads used (see Materials and Methods). The affinity of the RNA population for SL1 at each cycle was evaluated by EMSA at 4 °C. No shift of the target was seen at 10 μM for candidates issued from the first round of selection, whereas at the eighth round 50% of the target was shifted at 50 nM. No further evolution in terms of affinity to SL1 was observed between step 8 and step 10, and we proceeded to the cloning of the selected candidates.

Identification of Internal Loop-Containing RNA Aptamers. We analyzed 62 RNA candidates and obtained 12 different sequences. As is shown in Figure 1, a consensus sequence

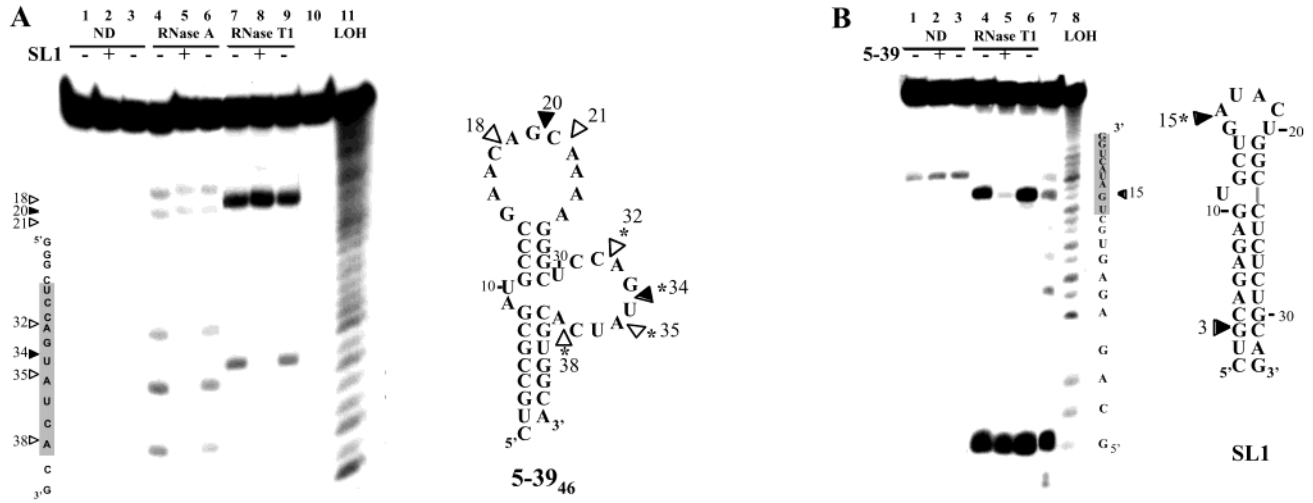

FIGURE 2: RNase probing of the SL1/5−39 complex. Analysis of the complex formed by the 5−39 aptamer and the SL1 hairpin obtained by using either the ^{32}P 3′-end-labeled 5−39$_{46}$ truncated aptamer (A) or the ^{32}P 5′-end-labeled SL1 hairpin (B), represented to the right of each autoradiography. Solid and open triangles on the primary sequences and secondary models indicate RNase T1 and RNase A cleavage sites, respectively. Asterisks refer to change of cleavage pattern in the presence of SL1 [for (A)] or 5−39 [for (B)]. (A) Lanes 1−3 represent nondigested RNA, lanes 4−6 represent RNA digested by RNase A, and lanes 7−9 represent RNA digested by RNase T1. Lane 11 corresponds to alkaline hydrolysis. The labeled RNA was either alone (lanes 1, 4, and 7; −), in the presence of an excess of SL1 (lanes 2, 5, and 8; +), or in the presence of an unrelated RNA molecule used as a control (lanes 3, 6 and 9; −). (B) Lanes 1−3 represent nondigested RNA, lanes 4−6 represent RNA digested by RNase T1, lane 7 corresponds to RNase T1 digestion of SL1 under denaturing conditions, and lane 8 corresponds to alkaline hydrolysis. The labeled RNA was either alone (lanes 1 and 4), in the presence of an excess of 5−39 (lanes 2 and 5), or in the presence of an unrelated RNA molecule used as a control (lanes 3 and 6).

(5′AGUAUC) complementary to 6 nt of the SL1 loop was present in 11 of them. The selected candidate (sequence 2−9, class C) which did not contain that consensus could potentially hybridize to 9 nt of the 3′ strand of the SL1 stem. The structure of each candidate was predicted using the mfold program (*27*, *28*).

On the basis of this analysis, selected anti-SL1 sequences were classified in three different classes, as illustrated in Figure 1: class A sequences presented the consensus sequence in an asymmetrical internal loop, whereas class B candidates presented it in the apical loop of a hairpin structure. Sequences belonging neither to A nor B classes formed class C. Further examination of class A sequences showed that the complementary internal loop was flanked on both sides by G-C-rich stems. For 2 out of 5 aptamers belonging to this family (aptamers 1−17 and 1−37) the internal loop was actually a bulge. Length and composition of the apical loop varied from one aptamer to another. We then evaluated the affinity for SL1 of the most representative candidates by EMSA at 37 °C. Aptamers presenting the SL1 complementary region in an internal loop (class A) had a higher affinity than those presenting it in an apical loop (class B). The aptamer 5−39, which bound SL1 with the highest affinity (70 nM under selection conditions), was chosen as a representative for investigating the properties of class A sequences.

Structure Probing of the SL1/5−39 Complex. On the basis of the primary sequence and the predicted structures, it was tempting to propose that the complex formed by SL1 and 5−39 involved an interaction between the apical loop of the target hairpin and the internal loop of the aptamer. Prior to mapping the interactions between 5−39 and SL1, the structures of individual molecules were probed with ribonucleases (Figure 2). Nucleotides in single-stranded regions were monitored with RNases T1 (G specific) and A (C and U specific). RNase digestions were performed at 37 °C in R buffer in order to maintain the same conditions as when the aptamer was selected. As we anticipated that interactions on the aptamer side might be restricted to the internal loop, we used a truncated version of the aptamer (5−39$_{46}$; Figure 3B), 46 nt long, which retained the binding capacity of the full-length aptamer. This made both the synthesis and the analysis easier.

Analysis of the RNase cleavage products of the ^{32}P 3′-end-labeled truncated aptamer 5−39$_{46}$ by denaturing polyacrylamide gel electrophoresis confirmed the secondary structure prediction (Figure 2A). In particular, strong RNase T1 and RNase A cleavages were detected in the apical loop (G^{20} for RNase T1, lane 7; C^{18} and C^{21} for RNase A, lane 4) and in the internal loop (G^{34} for T1, lane 7; C^{32}, U^{35}, and C^{38} for A, lane 4), indicating single-stranded regions. No cleavage of positions corresponding to the predicted double-stranded stem was detected (lanes 4 and 7). In the presence of SL1, cleavages corresponding to the internal loop disappeared, whereas the cleavage pattern corresponding to the apical loop remained mostly unchanged (lanes 5 and 8). The protection was specific as the cleavage pattern of 5−39$_{46}$ in the presence of an unrelated RNA hairpin (SL3 from the HCV 3′X region, lanes 6 and 9) did not change significantly from that of 5−39$_{46}$ alone. Therefore, the change of the cleavage pattern related to the association of 5−39$_{46}$ with SL1 indicated that SL1 interacted with the internal loop region of 5−39$_{46}$.

The same procedure was used with ^{32}P 5′-end-labeled SL1, and the result is shown in Figure 2B. The nondigested SL1 gave rise to two bands: one corresponding to the whole product and another one corresponding to a partial degradation at U^{17} (lane 1). This breakdown product was degraded upon RNase T1 treatment (lane 4). A prominent T1 cleavage was detected, corresponding to the apical loop (G^{15}) (lane 4), and weaker cleavages were detected in a longer exposure (not shown) at G^{8}, G^{10}, G^{12}, and G^{21}. Bands corresponding

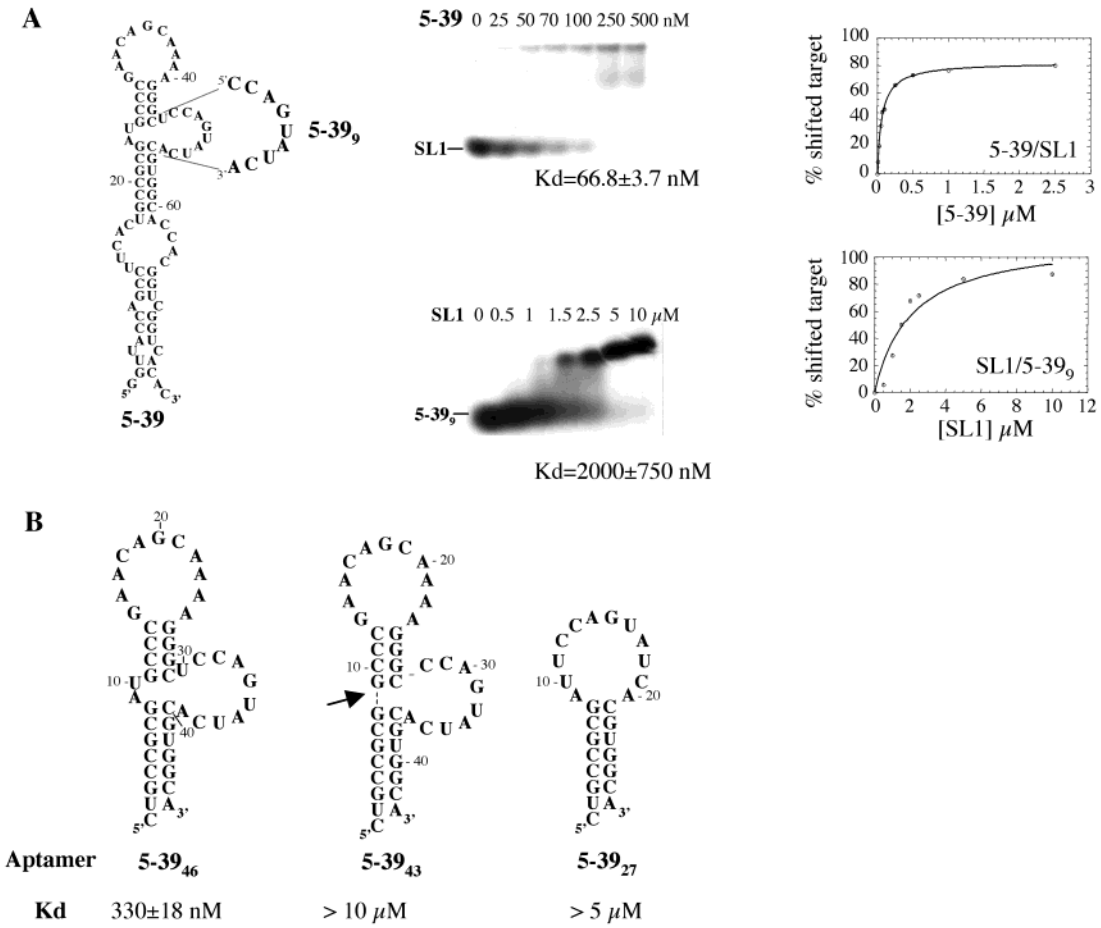

FIGURE 3: Electrophoretic mobility shift assay of 5−39 aptamer/SL1 complexes. (A) The 9 nt long oligonucleotide (5−39$_9$) corresponding to the complementary region to SL1 of the 5−39 aptamer is shown to the left. Electrophoretic mobility shift assays were performed at 37 °C as described in Materials and Methods. SL1 was labeled in assays with 5−39 (center top) whereas 5−39$_9$ was labeled in assays with SL1 (center bottom). The concentration of unlabeled partner is indicated at the top of each lane. The dissociation constant (determined from the binding curves shown to the right as explained in Materials and Methods) is indicated. (B) The secondary structure prediction of the different aptamer variants is shown. Binding constants obtained by band-shift assays are indicated to the bottom of each structure, below the aptamer name. The arrow on the 5−39$_{43}$ structure indicates deleted nucleotide.

to the latter cleavages and cleavage in G^{15} were abolished upon addition of the aptamer 5−39 (lane 5), indicating that the interaction takes place with the apical loop and part of the upper stem of SL1. In contrast, the presence of an unrelated RNA hairpin aptamer of the same size, selected against a different RNA stem−loop, did not change the cleavage pattern of SL1 (lane 6). A sensitive site (G^3) in the SL1 stem was not affected by the addition of either the aptamer or the control RNA. Taken together, these results confirm an apical loop−internal loop interaction of SL1 with the aptamer 5−39, a representative of class A aptamers.

Defining the Boundaries of the Anti-SL1 Aptamer. It was of interest to minimize the 5−39 oligomer and in particular to delineate the crucial elements accounting for the high affinity displayed toward SL1. To rule out the possibility that the affinity of 5−39 for SL1 was only due to the sequence of the internal loop complementary to the SL1 apical loop, we chemically synthesized the 9 nt long antisense oligoribonucleotide corresponding to the 5−39 region complementary to SL1 (Figure 3A). At 37 °C, i.e., the temperature at which selection was carried out, the antisense 9mer bound very poorly to SL1, with a K_d of about 2 μM in comparison to about 70 nM for the intact aptamer. These results indicate that besides hydrogen bonding between the internal loop of 5−39 and the apical loop of SL1, additional interactions contribute to the stability of the aptamer−SL1 complex.

As a means to determine the regions crucial for the formation of the SL1/5−39 complex, we analyzed the binding properties of truncated and mutated versions of 5−39 (Figure 3B). 5−39$_{46}$, lacking the lower part (roughly corresponding to the PCR primers), induced a shift of 50% of SL1 at 330 nM, i.e., a 5-fold decrease compared to the selected sequence. This shortened aptamer constituted the basis for investigating the role of either the apical or the internal loop. The deletion of the three nucleotides, in the internal loop, that were not complementary to SL1 (A^9, U^{10}, and U^{30}) led to an oligomer (5−39$_{43}$) which did no longer bind to SL1. The molecule lacking the upper stem−loop (5−39$_{27}$) was no longer able of inducing a shift of SL1 below 10 μM, thus indicating that a stable kissing complex cannot be formed with SL1 despite the presence of the consensus motif. The bimolecular aptamer resulting from the hybridization of two oligomers corresponding to the 5′ and to the 3′ strand of 5−39$_{46}$ (Figure 4) retained the binding properties of the monomolecular species (K_d of 48 nM in comparison to 150 nM for 5−39$_{46}$ at 4 °C). This demonstrated that the upper stem, but not the top loop, was important for binding, and this allowed us to combine different mutations and

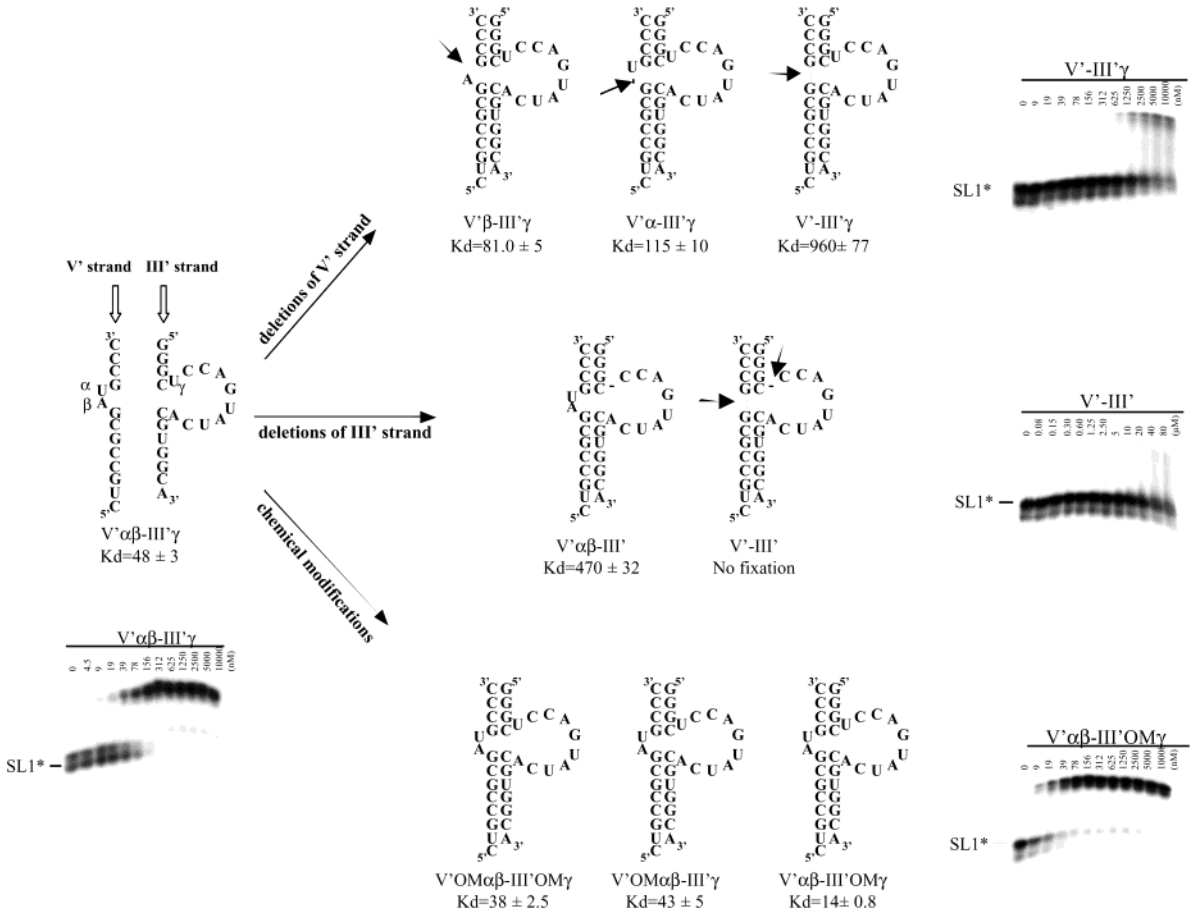

FIGURE 4: Bimolecular truncated aptamers derived from $5-39_{46}$. Oligomers V′αβ and III′γ correspond to the 5′ and 3′ strands of the $5-39_{46}$ aptamer. Greek letters indicate nucleotides in the internal loop that are not complementary to SL1 (U^{10} = α, A^9 = β, and U^{30} = γ). Oligomers were prepared either in the phosphodiester or in the 2′-*O*-methyl (OM) series. Eight variants of the bimolecular aptamer are shown to the right of the V′αβ−III′γ bimolecular aptamer. Arrows indicate deleted nucleotides. The dissociation constant of each bimolecular aptamer with SL1 is indicated in nanomolar at the bottom of each schematic representation. Some representative EMSAs are shown; the concentration of the unlabeled partner is indicated at the top of each lane.

different chemistries for each strand. As we expected from the results with the oligomer $5-39_9$, no shift of SL1 was seen at concentrations up to 10 μM of the 3′ strand alone (data not shown).

To analyze the role of the two unpaired nucleotides A^9 and U^{10} in the 5′ strand, named β and α, we synthesized four oligonucleotides containing both, either one, or none of them (V′αβ, V′α, V′β, and V′, respectively). Similarly, we synthesized two oligomers named III′γ and III′ corresponding to the 3′ strand with and without U^{30} (Figure 4). Electrophoretic mobility shift assays against SL1 at 4 °C were then performed using different combinations of all six oligonucleotides. Complexes formed by molecules in which the impaired nucleotides of the internal loop had been deleted bound poorly to SL1 compared to $5-39_{46}$. The combination V′−III′ corresponding to the triple deletion shifted only 30% of SL1 at concentrations up to 80 μM, in agreement with the behavior of $5-39_{43}$. The combination of one wild-type sequence with a strand in which the critical residues were removed (V′−III′γ or V′αβ−III′) had at least a 10-fold decreased association constant. When either A^9 or U^{10} is present, the stability of the complexes formed with the wild-type 3′ strand was only slightly affected (K_d of 80 and 115 nM, respectively).

2′-*O*-Methyl-substituted RNA oligomers are known to bind more strongly to RNA than unmodified RNA oligomers and are resistant to nucleases (*29*). We thus prepared the 2′-*O*-methyl (OM) versions of the wild-type strands of the bimolecular aptamer, generating three different molecules containing either one (V′OMαβ−III′γ or V′αβ−III′OMγ) or two modified strands (V′OMαβ−III′OMγ). Both V′OMαβ−III′γ and V′OMαβ−III′OMγ showed no significant improvement in their affinity to SL1 in comparison to the regular RNA complex V′αβ−III′γ, whereas the complex formed by V′αβ−III′OMγ had more than a 3-fold improved affinity.

Does the Complex SL1/5−39 Correspond to a Kissing Interaction? Loop−loop interactions have been described in RNA−RNA complexes between two hairpins with complementary loops (*3*, *30*−*32*). Such so-called "kissing" complexes are selectively recognized by the ROP protein of *E. coli* (*3*, *26*, *32*). We wondered whether this protein would recognize the ALIL complex. The small size of ROP did not allow us to see its interaction with the SL1/5−39 complex by EMSA. Studies of the SL1/5−39 complex were actually performed by surface plasmon resonance (SPR) using the chemically synthesized shortened version $5-39_{35}$ of the aptamer. This variant was obtained by substituting the apical loop of $5-39_{46}$ (from G^{15} to A^{25}) by a poly(ethylene glycol) tether and maintaining the 4 bp upper stem.

We immobilized on the sensorchip of the SPR equipment two different RNA hairpins: SL1 and miniTAR, a shortened

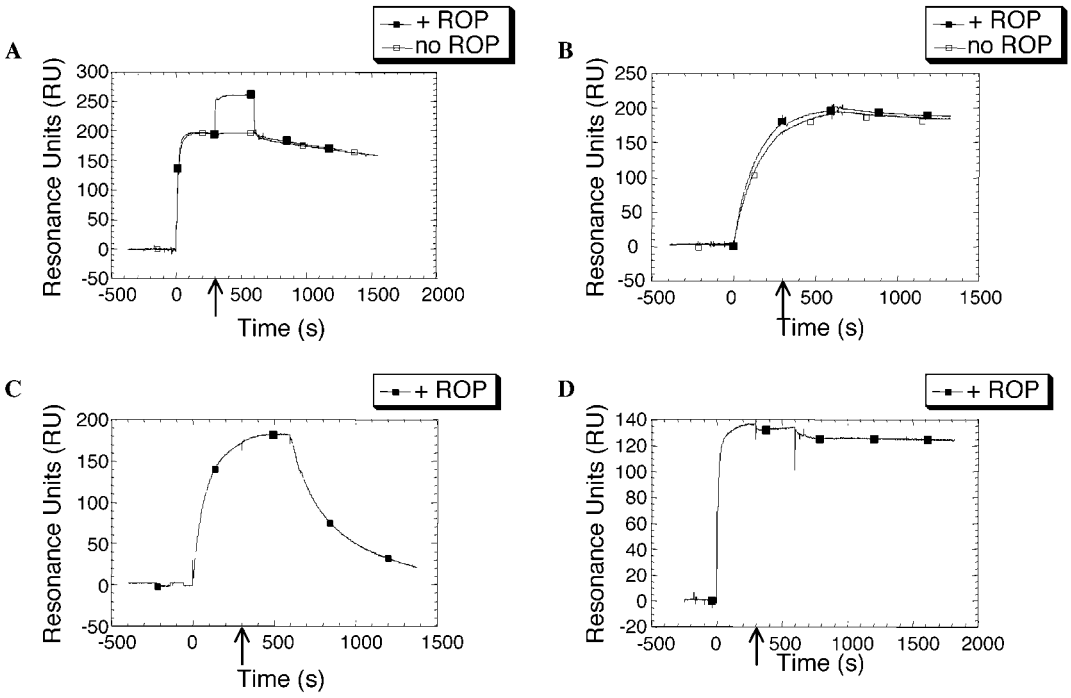

FIGURE 5: Sensorgrams of RNA hairpin/oligonucleotide complexes. Mini-TAR with anti-TAR RNA aptamer $R06_{24}$ (A), mini-TAR with anti-TAR DNA aptamer A21 (C), and mini-TAR with antisense oligoribonucleotide L2−17 (D); SL1 with $5-39_{35}$ (B) in the presence or absence of ROP. All experiments were performed with a constant concentration (1 μM) of the oligonucleotide injected for 600 s. Solid symbol: ROP (0.8 μM) was co-injected (arrow) with the oligonucleotide 300 s after the start of the continual injection of oligonucleotide. Empty symbol: the oligonucleotide was injected alone for 600 s (panels A and B).

version of the trans-activation response element (TAR) of human immunodeficiency virus 1 (HIV-1) with a double-stranded stem and a six-membered loop which was used in previous studies (*8*, *25*). When $5-39_{35}$ was injected, it bound to SL1 but not to miniTAR (Figure 5B); conversely, $R06_{24}$, an RNA hairpin aptamer selected against TAR RNA, previously shown to form a kissing complex with TAR (*8*), gives a signal on the mini TAR channel but not on the SL1 channel (Figure 5A). No fixation of ROP on the immobilized individual RNA stem−loops was observed (not shown). An increase of the resonance signal upon ROP injection was indicative of the formation of a ROP/mini TAR/$R06_{24}$ complex (Figure 5A). In contrast, no interaction of ROP was seen with the SL1/$5-39_{35}$ complex. No increase of the signal was seen with ROP on the mini TAR channel either when a DNA aptamer (A21) that forms a kissing complex with mini TAR (Sekkai et al., unpublished results) or when L2−17, an RNA antisense 17mer against miniTAR (*33*), was used (Figure 5C,D). Therefore, as ROP protein does not recognize the SL1/5−39 complex, the ALIL interaction is structurally different from the apical loop−apical loop interaction characteristic of the complex formed by two hairpins.

Analysis of Selected IRES IV Domain-Binding RNA Sequences. The selection of RNA aptamers against the HCV IRES IV domain, using a library of about 10^{12} oligoribonucleotides candidates, was performed by affinity capture of biotinylated RNA−aptamer complexes on streptavidin magnetic beads as described in Materials and Methods. After each cycle of selection, we analyzed the amount of domain IV bound to candidates by electrophoretic mobility shift assay under the selection conditions. No shift of the target was seen at 1 μM for candidates issued from the first and second round of selection, whereas at the seventh round 50% of the target was shifted at 180 nM. No further significant evolution of the population was observed at round 8, so we cloned and sequenced the selected candidates. Twenty-six out of 30 sequenced candidates displayed a consensus sequence, $^{5'}$AUCAUGG, complementary to the apical loop of domain IV (not shown). Interestingly, about 60% of them could be folded in a way similar to that described above for class A aptamers against SL1: the consensus heptameric motif was located in an internal loop flanked by two G-C-rich stems. All candidates presenting this structure were amplified and transcribed in vitro in order to evaluate their affinity for domain IV. EMSA performed with ^{32}P 5′-end-labeled domain IV led to a K_d of about 20 nM for the best aptamer, named IV-55 (Figure 6).

We mapped the complex formed by the aptamer IV-55 and domain IV of the HCV IRES by RNase digestion in the conditions of selection (23 °C in R buffer). The loop of the 5′-end-labeled domain IV was sensitive to RNases (Figure 7A): position G^{13} was cleaved by RNase T1 (lane 7) and positions U^{12}, C^{10}, and C^{9} were cleaved by RNase A (lane 4). In the presence of IV-55 (lanes 5 and 8), these bands corresponding to cleavage of the apical loop of domain IV were less intense, indicating that these positions were protected in the IRES loop IV/RNA−IV-55 aptamer complex. An RNase cleavage site located in the bottom part of the stem was not affected by the addition of the aptamer, indicating that the protection pattern was specific. Moreover, no protection was observed when digestion was performed in the presence of IIIe-4 (lanes 6 and 9), an RNA aptamer selected to specifically bind the IRES stem−loop IIIe (Tallet et al., unpublished results).

The 5′-end-labeled aptamer IV-55 was sensitive to RNases: positions C^{38} and C^{41} were cleaved by RNase A, and position G^{44} was cleaved by RNase T1 (Figure 7B, lanes 4 and 7). These cleavages are located in the internal loop of

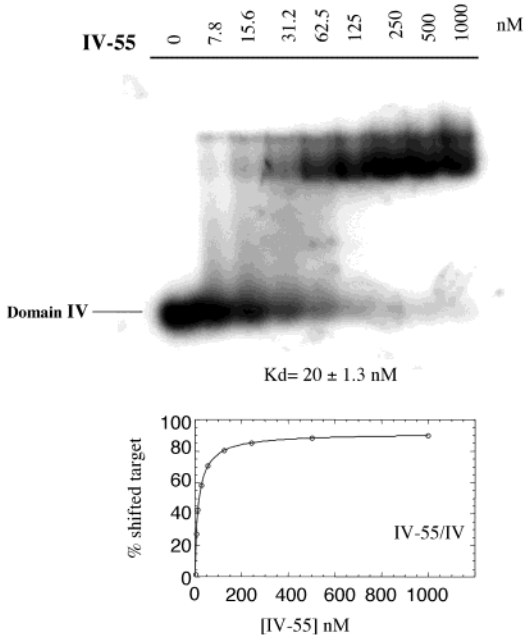

FIGURE 6: Analysis of the IV-55 aptamer/IV complex by electrophoretic mobility shift assay. Electrophoretic mobility shift assays were performed at 23 °C as described in Materials and Methods. Domain IV was 5′-end-labeled, and the concentration of unlabeled IV-55 is indicated at the top of each lane. The binding constant (determined as explained in Materials and Methods) was derived from the titration curve shown at the bottom part.

IV-55. In the presence of domain IV (lanes 5 and 8), these bands were less intense, showing that G^{44}, C^{38}, and C^{41} were protected in the IV-55/domain IV complex. No protection was observed when digestions were performed in the presence of the nonrelevant aptamer IIIe-4 (lanes 6 and 9). Minor bands can be visualized corresponding to G^{23}, G^{24}, G^{33}, and G^{34} cleavages by RNase T1, and these positions seem to be protected by the IV domain. This protection could be explained either by steric hindrance due to the complex formation or by a structural rearrangement of this part of the aptamer upon association to domain IV. In contrast, U^{29} was cleaved in the free aptamer and not protected by domain IV, showing that the apical loop of IV-55 was not involved in the complex formation. These results support an apical loop−internal loop interaction in the domain IV/IV-55 aptamer complex, similar to the one described above for the complex of the SL1 hairpin of the 3′X element and the 5−39 aptamer.

DISCUSSION

RNA aptamers selected against the SL1 hairpin from the 3′X element of the HCV mRNA contain 6−10 contiguous nucleotides complementary to the RNA target. In all but one case the antisense portion of the aptamer is complementary to the SL1 loop. The exception (aptamer 2−9), which could give rise to a 9 base pair duplex with the 3′ strand of the target hairpin, is characterized by a mediocre affinity (K_d > 10 μM) compared to the other selected candidates likely due to the competition with the 5′ strand of the stem. This validates our in vitro selection: this procedure identified that particular site, within the target RNA structure, at which the energy to be paid for making the complementary sequence available is the weakest. This might have been favored by the fact that the predicted apical loop of SL1 is closed by a G•U pair and that a bulged U residue disrupts the upper part of the stem. Faint bands detected on the RNase T1 footprint of SL1 (Figure 2B, lane 4), corresponding to cleavage at G^8, G^{10}, G^{12}, and G^{21}, actually suggest a transient opening of the region next to the loop. Such a dynamic structure might have permitted the invasion of the upper stem by the aptamer sequence. Indeed, most of the selected oligonucleotides show a sequence complementary to SL1 beyond the predicted apical loop (Figure 1). Most of the aptamers, and remarkably all those belonging to class A, share a $^{5'}$CCAGUAUC sequence; the 2 C's at the 5′ end could generate two GC pairs with the target RNA, which would compete out the G^{21}•U^{14} and G^{22}•C^{13} pairs of the SL1 stem.

However, the presence of a sequence complementary to the apical part of the SL1 stem does not fully account for the high affinity exhibited by the best aptamers. First, even though, as stated above, most of the aptamers display the octameric antisense consensus, the dissociation constant ranges from 70 nM to >1.3 μM. Second, the nonamer $5-39_9$, equivalent to the antisense part of the aptamer 5−39, is a poor binder compared to the authentic selected sequence (Figure 3A). Third, the 3′ half of 5−39 (III′γ), which includes the motif antisense to SL1, is even a weaker SL1 ligand than $5-39_9$ (Figure 4), likely because of the electrostatic repulsion due to the unpaired stretches flanking the complementary region. Fourth, even a sequence (aptamer 1−1) susceptible to generate 10 base pairs, including a G•U pair, binds more than 10 times less efficiently than 5−39, which can potentially form 9 base pairs. One major difference between these two different aptamers resides in their secondary structure. In class A as well as class B aptamers the consensus sequence is located in a loop, whereas in class C it is involved (at least in part) in a double-stranded region as predicted by mfold. Therefore, as previously observed for anti-TAR and anti-$tRNA^{Phe}$ RNA aptamers (*25*, *34*), the context in which the antisense sequence is presented is of key importance.

In these previous studies, the consensus aptamer was a hairpin structure whose apical loop was fully complementary to the loop of the target structure, thus giving rise to a loop−loop (kissing) complex. In the present study, the selected hairpins (class B aptamers) showing a loop complementary to the SL1 loop and susceptible to kiss led to complexes of moderate stability compared to those identified against TAR (*8*, *25*). Moreover, in contrast to the selection carried out against the TAR element, RNA hairpins were not the strongest selected ligands of SL1. We notice that the predicted SL1 loop is A,U-rich whereas the TAR one ($^{5'}$-AGGGUC) is G,C-rich. In addition, if we assume that the upper part of the SL1 stem has a single-stranded character, the SL1 hairpin might be better seen with a loop larger than eight nucleotides. Natural and artificial RNA−RNA kissing complexes characterized so far between hairpins with fully complementary loops involve six- to seven-membered loops (*30*, *35*, *36*). Such complexes are depicted as very tight complexes with a single phosphodiester unit connecting the loop−loop helix to either hairpin stem. Enlarging the complementary loops will lead to longer "kissing helices" whose end to end spanning will require longer connectors. Kissing complexes involving loops longer than six to seven nucleotides have been described for the dimerization initiation sites of retroviral RNA (*31*, *37*, *38*). However, in this

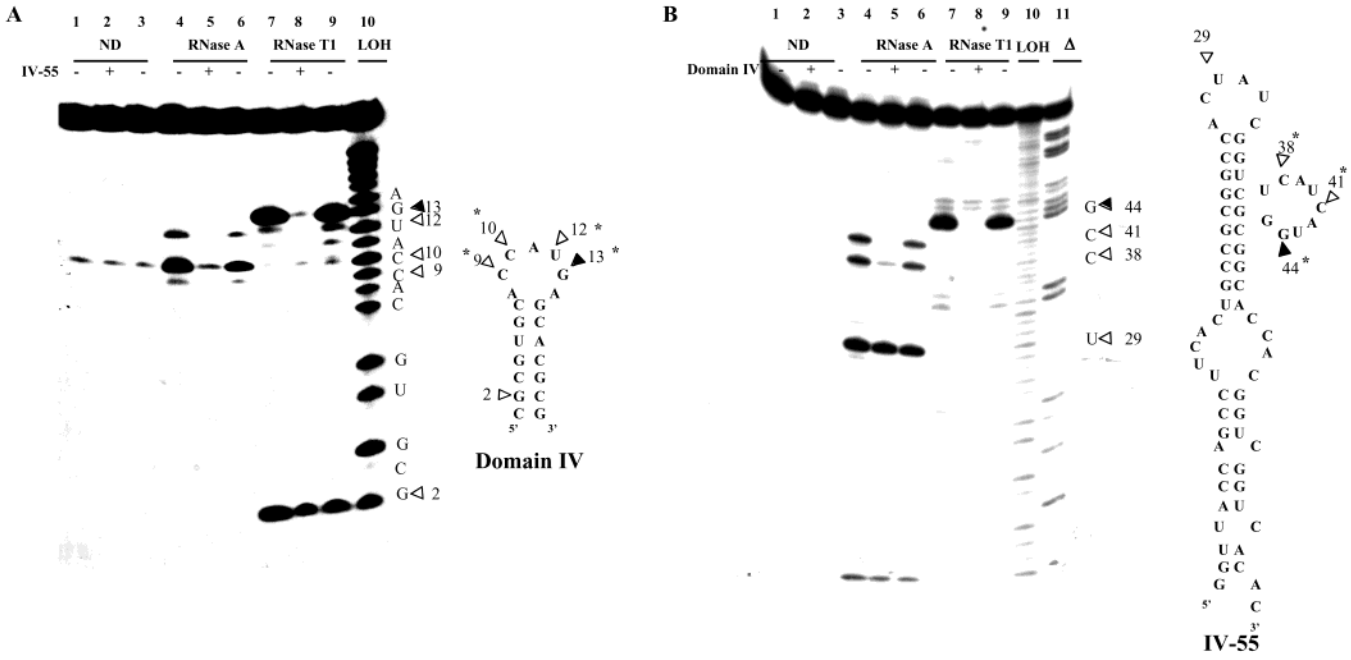

FIGURE 7: RNase probing of the domain IV/IV-55 complex. Analysis of the complex formed by the aptamer IV-55 and domain IV obtained by using either the ^{32}P 5′-end-labeled domain IV (A) or the ^{32}P 5′-end-labeled IV-55 aptamer (B), represented to the right of each autoradiography. Lanes 1−3 represent nondigested RNA. Lanes 4−6 represent RNA digested by RNase A, and lanes 7−9 represent RNA digested by RNase T1. The labeled RNA was either alone (lanes 1, 4, and 7; −), in the presence of its partner (lanes 2, 5, and 8; +), or in the presence of an unrelated RNA molecule used as a control (lanes 3, 6, and 9; −). Solid triangles on the primary and secondary models indicate RNase T1, and open triangles indicate RNase A cleavage sites, respectively. Asterisks refer to change of cleavage pattern in the presence of aptamer IV-55 [for (A)] or domain IV [for (B)]. Lanes 10 and 11 correspond to alkaline hydrolysis and RNase T1 digestion of RNAs under denaturing conditions, respectively.

case the 9 nt long loops are not fully complementary and generate a transient 6 base pair kissing complex evolving toward an extended duplex.

Whatever the reason, aptameric hairpins (class B) which could potentially form kissing complexes with the SL1 hairpin were not the ligands displaying the highest affinity identified by in vitro selection. Instead, class A aptamers characterized by an imperfect stem−loop structure with an internal loop complementary to the SL1 apical loop yield high-affinity complexes. Indeed, converting the 5−39 aptamer into the $5-39_{27}$ hairpin whose loop contained the nonameric sequence complementary to the top part of SL1 resulted in a drastic reduction of the binding constant (Figure 3B). Therefore, displaying the sequence complementary to the apical loop of SL1 in a internal loop provides the aptamer with an advantage for binding. Such aptamers have been selected in the presence of 3 mM Mg^{2+}. Different shapes might have been identified under different conditions. Previous studies have demonstrated that RNA hairpin−DNA aptamer interactions were modulated by magnesium concentration (Sekkai et al., unpublished). Similarly, kissing complexes formed by RNA aptamers with the TAR element of HIV-1 were strongly dependent on Mg^{2+} (*25*).

Footprinting analysis of SL1/5−39 complex actually demonstrates an apical loop (SL1)−internal loop (5−39) interaction (Figure 2). This ALIL complex might involve up to 9 base pairs which would require the disruption of at least 2 base pairs of the predicted SL1 stem, next to the loop. Interestingly, two C's are present in all 25 sequences at positions susceptible to pair with the two G's at the top of the 5′ strand of the SL1 stem (Figure 1). The length of the ALIL helix may vary from 8 to 10 nucleotides depending on the class A aptamer. All selected class A sequences show G,C-rich upper and lower stems surrounding the central loop. The presence of the two stems is crucial for stable complex formation: (i) shortening the lower helix reduces the SL1/5−39 binding constant and (ii) deleting the upper stem abolishes the complex. Assuming a 9 bp helix for the SL1/5−39 complex (Figure 8), the connection of the ALIL helix to the lower and upper stem of 5−39 will require a few residues: at least one nucleotide is necessary on each side of the upper helix (U^{30} and either A^9 or U^{10}) as demonstrated by the analysis of bimolecular aptamer variants (Figure 4). Similarly, according to the same model (Figure 8) the 3′ end of the 5′ strand of the SL1 stem is connected to the entrance of the ALIL helix through a single nucleotide unit (C^{13}). This is in fair agreement with the distance to be spanned over the major groove of A-type helices resulting from the interaction between two RNA loops (*39*). In contrast, the apical loop of the aptamer is dispensable. First, both the sequence and the length vary from one aptamer to the other within class A. Second, both the $5-39_{35}$ variant in which the apical loop has been substituted by a nonnucleotide linker (Figure 5) and bimolecular derivatives resulting from the association of oligomers corresponding to the 3′ and 5′ strand of 5−39 retain the capacity to bind to SL1 (Figure 4).

Similar aptamers have been independently identified by in vitro selection of RNA ligands against the hairpin corresponding to domain IV of the HCV IRES. Preliminary binding assays and footprinting analysis support ALIL interactions in the domain IV/aptamer IV-55 complex. Interestingly, the predicted secondary structure of IV-55 shows no single-stranded residue in the strand opposite to the internal loop (Figure 8). But three nucleotides remain

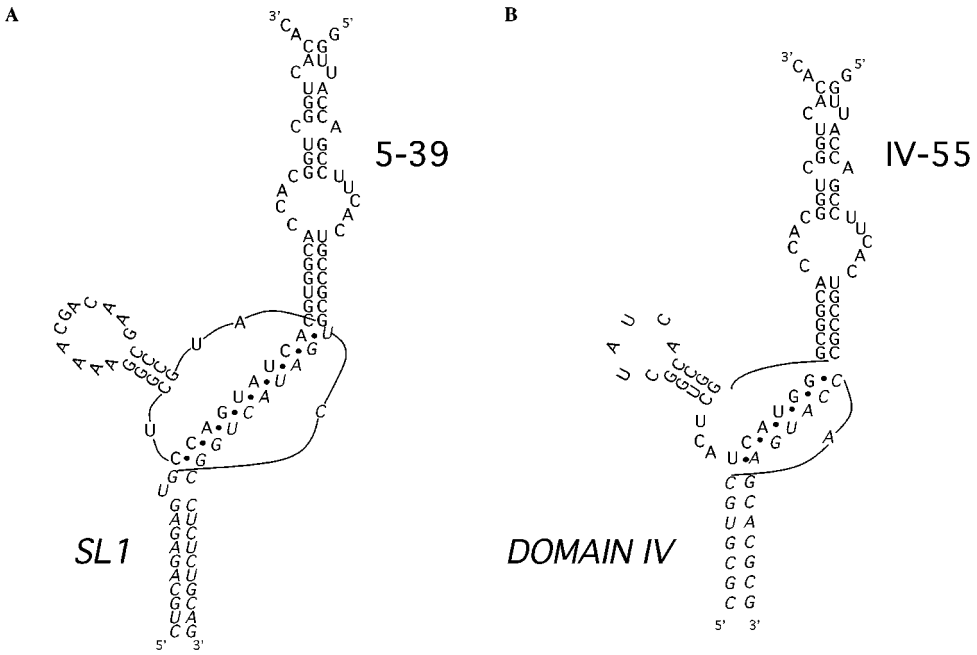

FIGURE 8: Scheme of the proposed ALIL interaction. The aptamers are shown in bold characters, and the hairpin targets are italicized. The proposed interactions between the aptamer internal loop and the hairpin target apical loop are indicated by ●. (A) 5−39 RNA aptamer/SL1 hairpin complex. (B) IV-55 RNA aptamer/domain IV complex.

impaired in the aptamer loop, leading to a connector length equivalent to that of the SL1/5−39 complex (Figure 8).

Interestingly, ALIL interactions have been described for the formation of specific bicoid mRNA−Staufen protein complexes, which is required for determining the correct anteroposterior polarity of the *Drosophila* embryo (*40*). The association of the protein to the mRNA requires intermolecular base pairing between an apical loop and an internal loop which could generate a 6 bp duplex. It should be pointed out that the internal loop of the bicoid mRNA involved in this complex is flanked on each side by three GC pairs. Therefore, in vitro selection allowed the identification of RNA elements of interest for higher order organization of natural RNAs.

The binding properties of the selected sequences, together with the function played by domain IV of the HCV IRES and the SL1 hairpin of the HCV 3′X region in the translation of the HCV mRNA, led us to investigate the effect of the aptamers 5−39 and IV-55 on in vitro protein synthesis. Preliminary results obtained using a dicistronic luciferase construct, in which the renilla gene was framed by the IRES and by the 3′X region of HCV, show that the anti-3′X aptamer 5−39 was without any effect on translation, whereas the anti-domain IV aptamer IV-55 was a selective inhibitor in the high nanomolar range.

Presently, the structure of ALIL complexes is not elucidated. Even though loop−loop interactions are concerned, the ALIL complex should be structurally different from the intermolecular complexes involved in the control of DNA replication (*35*) and in the TAR RNA−aptamer interaction (*25*) as the SL1/5−39 complex is not recognized by ROP, which is specific for kissing complexes. The elucidation of the structure of the ALIL complex which might be relevant for natural RNA−RNA inter- or intramolecular complexes is in progress.

ACKNOWLEDGMENT

We are deeply grateful to Justine Michel for oligomer synthesis. We thank Claudine Boiziau for helpful discussions about RNase probing. We acknowledge the contribution of Christian Cazenave in expressing and purifying the ROP protein. We are indebted to Annie Cahour for the dicistronic plasmids used in this work.

REFERENCES

1. Borer, P. N., Lin, Y., Wang, S., Roggenbuck, M. W., Gott, J. M., Uhlenbeck, O. C., and Pelczer, I. (1995) *Biochemistry 34*, 6488−6503.
2. Mao, H., White, S. A., and Williamson, J. R. (1999) *Nat. Struct. Biol. 6*, 1139−1147.
3. Eguchi, Y., and Tomizawa, J. (1990) *Cell 60*, 199−209.
4. Hélène, C., and Toulmé, J. J. (1990) *Biochim. Biophys. Acta 1049*, 99−125.
5. Tuerk, C., and Gold, L. (1990) *Science 249*, 505−510.
6. Ellington, A. D., and Szostak, J. W. (1990) *Nature 346*, 818−822.
7. Boiziau, C., Dausse, E., Yurchenko, L., and Toulmé, J. J. (1999) *J. Biol. Chem. 274*, 12730.
8. Ducongé, F., and Toulmé, J. J. (1999) *RNA 5*, 1605−1614.
9. Tanaka, T., Kato, N., Cho, M. J., and Shimotohno, K. (1995) *Biochem. Biophys. Res. Commun. 215*, 744−749.
10. Tanaka, T., Kato, N., Cho, M. J., Sugiyama, K., and Shimotohno, K. (1996) *J. Virol. 70*, 3307−3312.
11. Kolykhalov, A. A., Feinstone, S. M., and Rice, C. M. (1996) *J. Virol. 70*, 3363−3371.
12. Blight, K. J., and Rice, C. M. (1997) *J. Virol. 71*, 7345−7352.
13. Blackwell, J. L., and Brinton, M. A. (1995) *J. Virol. 69*, 5650−5658.
14. Rice, C. M. (1996) in *Fields Virology* (Fields, B. N., Knipe, D. M., and Howley, P. M., Eds.) Raven Publishers, Philadelphia, PA.
15. Ito, T., and Lai, M. M. (1997) *J. Virol. 71*, 8698−8706.
16. Oh, J. W., Ito, T., and Lai, M. M. (1999) *J. Virol. 73*, 7694−7702.
17. Ito, T., Tahara, S. M., and Lai, M. M. (1998) *J. Virol. 72*, 8789−8796.

18. Yanagi, M., St. Claire, M., Emerson, S. U., Purcell, R. H., and Bukh, J. (1999) *Proc. Natl. Acad. Sci. U.S.A. 96*, 2291−2295.
19. Bukh, J., Purcell, R. H., and Miller, R. H. (1992) *Proc. Natl. Acad. Sci. U.S.A. 89*, 4942−4946.
20. Reynolds, J. E., Kaminski, A., Carroll, A. R., Clarke, B. E., Rowlands, D. J., and Jackson, R. J. (1996) *RNA 2*, 867−878.
21. Rijnbrand, R., Bredenbeek, P., van der Straaten, T., Whetter, L., Inchauspe, G., Lemon, S., and Spaan, W. (1995) *FEBS Lett. 365*, 115−119.
22. Kamoshita, N., Tsukiyama-Kohara, K., Kohara, M., and Nomoto, A. (1997) *Virology 233*, 9−18.
23. Wang, C., Sarnow, P., and Siddiqui, A. (1993) *J. Virol. 67*, 3338−3344.
24. Honda, M., Ping, L. H., Rijnbrand, R. C., Amphlett, E., Clarke, B., Rowlands, D., and Lemon, S. M. (1996) *Virology 222*, 31−42.
25. Ducongé, F., Di Primo, C., and Toulmé, J. J. (2000) *J. Biol. Chem. 275*, 21287−21294.
26. Predki, P. F., Nayak, L. M., Gottlieb, M. B., and Regan, L. (1995) *Cell 80*, 41−50.
27. Zuker, M., Mathews, D. H., and Turner, D. (1999) in *RNA Biochemistry and Biotechnology* (Clark, J. B. B. F. C., Ed.) pp 11−43, Kluwer Academic Publishers, Dordrecht, The Netherlands.
28. Mathews, D. H., Sabina, J., Zuker, M., and Turner, D. H. (1999) *J. Mol. Biol. 288*, 911−940.
29. Inoue, H., Hayase, Y., Imura, A., Iwai, S., Miura, K., and Ohtsuka, E. (1987) *Nucleic Acids Res. 15*, 6131−6148.
30. Gregorian, R. S., Jr., and Crothers, D. M. (1995) *J. Mol. Biol. 248*, 968−984.
31. Clever, J. L., Wong, M. L., and Parslow, T. G. (1996) *J. Virol. 70*, 5902−5908.
32. Comolli, L. R., Pelton, J. G., and Tinoco, I., Jr. (1998) *Nucleic Acids Res. 26*, 4688−4695.
33. Ecker, D. J., Vickers, T. A., Bruice, T. W., Freier, S. M., Jenison, R. D., Manoharan, M., and Zounes, M. (1992) *Science 257*, 958−961.
34. Scarabino, D., Crisari, A., Lorenzini, S., Williams, K., and Tocchini-Valentini, G. P. (1999) *EMBO J. 18*, 4571−4578.
35. Tomizawa, J. I., and Itoh, T. (1981) *Proc. Natl. Acad. Sci. U.S.A. 78*, 6096−6100.
36. Chang, K. Y., and Tinoco, I., Jr. (1994) *Proc. Natl. Acad. Sci. U.S.A. 91*, 8705−8709.
37. Skripkin, E., Paillart, J. C., Marquet, R., Ehresmann, B., and Ehresmann, C. (1994) *Proc. Natl. Acad. Sci. U.S.A. 91*, 4945−4949.
38. Muriaux, D., Foose, P., and Paoletti, J. (1996) *Biochemistry 35*, 5075−5082.
39. Haasnoot, C. A. G., Hilbers, C. W., Van der Marel, G. A., Van Boom, J. H., Singh, U. C., Pattabiraman, N., and Kollman, P. A. (1986) *J. Biomol. Struct. Dyn. 3*, 843−855.
40. Ferrandon, D., Koch, I., Westhof, E., and Nusslein-Volhard, C. (1997) *EMBO J. 16*, 1751−1758.

BI0121508